Sains Malaysiana 55(3)(2026): 561-571
http://doi.org/10.17576/jsm-2026-5503-16

Discriminating Walrus and Narwhal Tusks through Integrated Biomineralogical and Geochemical Analysis

(Membezakan Gading Walrus dan Narwhal melalui Gabungan Analisis Biomineralogi dan Geokimia)

LU XINGYU & AZIMAH HUSSIN*

Geology Program, Department of Earth Science and Environment, Faculty of Science and Technology, Universiti Kebangsaan Malaysia, 43600 UKM Bangi, Selangor, Malaysia

Received: 29 August 2025/Accepted: 4 March 2026

ABSTRACT

Marine ivory, derived primarily from walrus (*Odobenus rosmarus*) and narwhal (*Monodon monoceros*) tusks, is a culturally and economically significant but vulnerable resource. Effective regulation of its trade requires reliable and non-destructive methods for species identification, yet current approaches remain limited. This study systematically compares the mineralogical, microstructural, and geochemical characteristics of walrus and narwhal tusks using an integrated suite of analytical techniques, including SEM, XRD, Raman spectroscopy, EDX and XRF analysis. Results based on SEM, Raman spectroscopy, XRD, and XRF analyses show distinct diagnostic features: narwhal tusks exhibit tightly bound collagen fibers interwoven with elongated hydroxyapatite crystals and fine, uniform porosity, whereas walrus tusks display disordered crystal clusters, partial collagen degradation, and more pronounced porosity. Both tusks are dominated by carbonate-substituted hydroxyapatite, but XRD and Raman results indicate that walrus apatite crystals are larger, more crystalline, and show stronger fluoride substitution. XRF and EDX data further indicate species-specific elemental signatures, with elevated Na_2O, MgO, Al_2O_3, SiO_2, and SrO in walrus, and enriched Sb and Cd in narwhal. A novel discriminant criterion derived from quantitative XRF measurements based on the Al_2O_3/P_2O_5 ratio (threshold $R_0 = 0.0033$) reliably distinguishes the two species. These findings establish a robust, non-destructive framework for forensic identification of marine ivory, offering direct applications to wildlife law enforcement, trade monitoring, and cultural heritage conservation.

Keywords: Geochemical analysis; mineralogical characteristics; narwhal tusk; organic gemstone; walrus tusk

ABSTRAK

Gading marin yang diperoleh terutamanya daripada gading walrus (*Odobenus rosmarus*) dan narwhal (*Monodon monoceros*), merupakan sumber yang signifikan dari segi kebudayaan dan ekonomi tetapi dalam masa yang sama terdedah kepada ancaman. Pengawalseliaan perdagangan yang berkesan memerlukan kaedah yang boleh dipercayai serta tidak merosakkan untuk pengecaman spesies, namun pendekatan sedia ada masih terbatas. Kajian ini secara sistematik membandingkan cirian mineralogi, mikrostruktur dan geokimia gading walrus dan narwhal melalui penggunaan gabungan teknik analisis. Hasil kajian berdasarkan analisis SEM, spektroskopi Raman, XRD dan XRF mendedahkan ciri diagnostik yang jelas: gading narwhal memperlihatkan serat kolagen yang terikat rapat dan saling berjalin dengan kristal hidroksiapatit berbentuk memanjang serta keliangan yang halus dan seragam, manakala gading walrus menunjukkan kelompok kristal yang tidak teratur, degradasi separa kolagen dan keliangan yang lebih ketara. Kedua-dua jenis gading didominasi oleh hidroksiapatit yang digantikan dengan karbonat, namun hasil XRD dan Raman menunjukkan bahawa kristal apatite dalam gading walrus adalah lebih besar, lebih berhablur dan memperlihatkan penggantian fluorida yang lebih kuat. Data XRF dan EDX seterusnya menunjukkan pengenalan unsur khusus spesies dengan kepekatan Na_2O, MgO, Al_2O_3, SiO_2 dan SrO yang lebih tinggi dalam gading walrus, manakala gading narwhal diperkaya dengan unsur Sb dan Cd. Satu kriteria pembezaan baharu berasaskan pengukuran kuantitatif XRF menggunakan nisbah Al_2O_3/P_2O_5 (ambang $R_0 = 0.0033$) dapat membezakan kedua-dua spesies dengan berkesan. Keputusan ini mewujudkan satu rangka kerja pengenalpastian forensik gading marin yang mantap serta tidak merosakkan dengan aplikasi langsung dalam penguatkuasaan undang-undang hidupan liar, pemantauan perdagangan dan pemuliharaan warisan budaya.

Kata kunci: Analisis geokimia; cirian mineralogi; gading narwhal; gading walrus; permata organik

INTRODUCTION

Tusks, particularly those of walrus and narwhal, represent a distinctive form of marine ivory derived from biological mineralization. Throughout human history, such tusks have played an enduring role in material culture, serving as raw materials for tools, ornaments, and symbolic objects. Archaeological evidence indicates that the utilization of tusk-derived ivory can be traced back to the Stone Age, exemplified by the 30,000-year-old 'Lion Man' figurine carved from mammoth ivory in Germany (Tranchant et al. 2023). In Arctic regions, walruses and narwhals have long provided important sources of *marine ivory*. Walruses (pinnipeds) develop elongated tusks in both sexes, with males exhibiting prominent canines exceeding one meter for use in combat and locomotor support, while females produce shorter tusks. Narwhals (*Monodon monoceros*), in contrast, are odontocetes characterized by a single, spiralled maxillary tusk measuring up to 2-3 m. Recent morphometric work has quantified the average spiral angle of narwhal tusks at ~67°, underscoring their unique morphology (Kiladze & Chernova 2018).

Historically, narwhal tusks were misidentified as 'unicorn horns' in European courts, celebrated as miraculous objects worth many times the weight of gold. In East Asia, powdered tusk material was incorporated into traditional medicines for protection against poison and malign spirits (Dąsal et al. 2021). Walrus tusks, conversely, were integral to indigenous Arctic lifeways for crafting utilitarian and ceremonial artifacts, and during the medieval period became an important ivory source traded into Europe.

Marine ivories are less studied than terrestrial ivories, such as elephant and mammoth ivory, despite their cultural and economic significance. Research on elephant and mammoth ivory has yielded well-established diagnostic methods. Schreger line analysis differentiates extant elephant ivory (angles >100°) from extinct mammoth ivory (angles <100°). Meanwhile, geochemical studies show distinct trace element differences for instance, marine mammal ivory exhibits fluoride concentrations in the order of thousands of ppm compared to tens to hundreds of ppm in modern elephant ivory (Locke 2008; Sims, Baker & Hoesch 2011). By contrast, systematic investigations of walrus and narwhal tusks remain limited, particularly in terms of mineralogy, microstructure, and chemistry (Sastri et al. 2013).

This knowledge gap has significant implications. Under the Convention on International Trade in Endangered Species of Wild Fauna and Flora (CITES) regulations, international trade in ivory is strictly controlled, requiring scientific forensic methods to distinguish between species. Cultural heritage studies also require reliable identification of ivory artifacts to establish authenticity and provenance. Conventional macroscopic methods, such as texture observation, are often destructive or inconclusive, while spectroscopic approaches (Raman analysis) can be hindered by fluorescence backgrounds and diagenetic alterations in archaeological materials (Edwards & O'Connor 2012). Well-documented cases, such as contentious identifications of ivory grave goods from Anglo-Saxon contexts, illustrate the challenges in differentiating elephant, walrus, and mammoth ivory without advanced analytical protocols (Hemer et al. 2023).

To address this gap, the present study systematically characterizes walrus and narwhal tusks using a combination of Scanning Electron Microscopy with Energy-Dispersive X-ray Spectroscopy (SEM-EDX), X-ray Diffraction (XRD), X-ray Fluorescence (XRF), and Raman spectroscopy. These methods collectively resolve microstructural morphology, mineral phases, bulk chemical composition, and molecular vibrational characteristics. By integrating these datasets, we aim to clarify the mineralogical and geochemical differences between walrus and narwhal ivory, thereby advancing the identification of marine ivory, supporting heritage conservation, and contributing to enforcement against the illegal ivory trade.

MATERIALS AND METHODS

This study uses a multi-analytical approach to compare narwhal and walrus tusk specimens. Twenty partial cross-sections were examined, including ten narwhal (N1–N10) and ten walrus (W1–W10) tusks. All specimens were by-products of traditional subsistence hunting by indigenous communities in the Russian Far East and were legally obtained from historical stockpiles under exemptions for indigenous cultural practices permitted by International Conventions. Representative photographs are shown in Figure 1.

Analytical characterization was conducted using Field Emission Scanning Electron Microscopy with Energy-Dispersive X-ray Spectroscopy (FESEM-EDX), X-ray Diffraction (XRD), X-ray Fluorescence (XRF), and Raman Spectroscopy. All analyses were performed at the Institute of Climate Change and Impact Research (ICRIM) Laboratory, Universiti Kebangsaan Malaysia (UKM). For microstructural and elemental analysis, FESEM-EDAX was used. Samples were carbon-coated to minimize charging effects, and imaging was performed at 2,000×–10,000× magnification to document dentine morphology. Elemental distributions were determined through calibrated point and area EDAX analyses with parameters optimized for key element quantification. XRD was used to determine the crystalline phases of powdered samples (<74 μm), scanned in the 2θ range of 5°–60° under standard operating voltages and currents. Phase identification was achieved by matching diffractograms against the ICDD PDF-4+ database.

XRF analysis of pressed powder pellets provided quantitative bulk chemical compositions. Calibration used certified reference materials, and a helium purge enhanced detection of light elements, achieving detection limits as

low as 15 ppm. Raman spectroscopy was performed with a 532 nm excitation laser (focused to approximately 1 µm), acquiring spectra within 200-3,200 cm^{-1}. The collected data were processed to resolve molecular vibrations and crystallographic phases with high accuracy. This integrated analytical workflow enabled comprehensive assessment of the microstructure, mineralogy, and chemical composition of narwhal and walrus tusks.

RESULTS AND DISCUSSION

PHYSICAL APPEARANCE

The narwhal tusk samples (Figure 1) show a smooth, creamy-yellow surface with faint internal bands and few surface marks. Their cross-sections are uniform, dense, and free of major cracks or dark spots. These characteristics are consistent with previous studies describing narwhal ivory as primarily dentine, with tight spiral growth, low porosity, and a pale color due to minimal secondary dentine or contamination (Locke 2008; Su & Cui 1999). Because of this fine texture and lack of marbling, narwhal ivory is highly valued for polished, gem-like ornamental work (Grandfield et al. 2014). The walrus tusk samples (Figure 1), by contrast, show pronounced marbling and darker cloudy spots, with greater variation in both color and structure. These patterns result from the mix of primary dentine and secondary dentine (osteodentine), which create an 'oatmeal-like' or mottled appearance (Mamaladze & Ustiashvili 2010). Long cracks and irregularities are also visible, serving as reliable diagnostic features of walrus ivory. Although this reduces its gem quality compared to narwhal tusks, the distinctive marbling is useful for identifying origin and authenticating artifacts (Darwent & LeMoine 2021).

In summary, narwhal ivory is smooth, pale, uniform, and ideal for gem carving and ornamentation. Walrus ivory, with its marbling, cracks, and mottling, is less favorable for gem-quality applications but valued for decorative carving, where its natural patterns are appreciated. Published guides confirm that narwhal tusks are identified by their spiral growth, clean color, and a relatively homogeneous internal texture, while walrus tusks show cementum layers, concentric rings, and prominent secondary dentine (Kiladze & Chernova 2018; Silaev et al. 2025). In the present samples, these physical characteristics clearly distinguish the two materials and indicate their different uses in gem and decorative arts.

GEOCHEMISTRY

XRF analysis shows that the bulk chemical compositions of both narwhal and walrus tusks are dominated by a hydroxyapatite matrix ($Ca_5(PO_4)_3(OH)$), with CaO contents

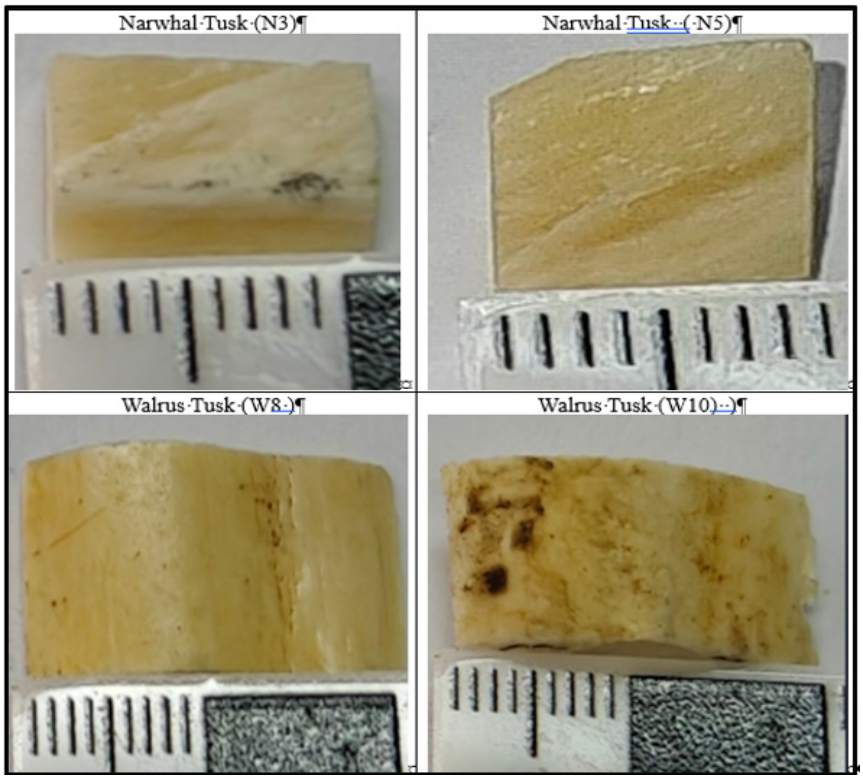

FIGURE 1. Comparison of narwhal (N3, N5) and walrus (W8, W10) tusks. Narwhal ivory is smooth, pale, and fine-textured, while walrus ivory is marbled, mottled, and structurally varied highlighting key traits for identification

ranging from 60-62 wt.% and P_2O_5 contents between approximately 33-34 wt.% (Figure 2). Narwhal tusks exhibit a slightly higher mean P_2O_5 content (33.86 wt.%) compared to walrus tusks (32.87 wt.%), whereas walrus tusks show a marginally lower mean CaO content (60.66 wt.%) than narwhal tusks (61.71 wt.%). In addition, XRF results indicate that walrus tusks contain markedly higher concentrations of Na_2O (1.875 wt.%), MgO (1.649 wt.%), SrO (0.108 wt.%), Al_2O_3 (0.325 wt.%), and SiO_2 (0.702 wt.%) than narwhal tusks (Na_2O 1.639 wt.%, MgO 1.146 wt.%, SrO 0.078 wt.%, Al_2O_3 0.049 wt.%, SiO_2 0.113 wt.%).

SEM–EDX analysis further confirms elemental differences at the microscale (Figure 3), showing enrichment of magnesium in walrus tusk (0.8 wt.%) relative to narwhal tusk (0.5 wt.%). In contrast, sodium contents measured by EDX partially overlap between the two materials, indicating that Na alone is insufficient as a single discriminant. Major elements such as Ca and P display comparable abundances in both tusk types, consistent with their shared calcium phosphate mineralogy.

Regarding sulfate and chloride, walrus tusk exhibits a mean SO_3 content of 0.99%, significantly higher than that of narwhal tusk (0.52%), while its chlorine (Cl) content (0.348%) is lower than that of narwhal tusk (0.490%). These differences likely reflect variations in their respective marine environments and associated geochemical adsorption or deposition processes. Although ZnO levels remain low in both materials (< 0.12%), walrus tusk has a slightly higher mean ZnO (0.104%) than narwhal tusk (0.066%) and show greater variability (standard deviations of 0.119% vs. 0.025%) (Hoelzig et al. 2020; Nganvongpanit et al. 2016a). Overall, walrus tusk demonstrates higher and more variable concentrations of alkali metals (Na_2O, MgO), trace impurities (Al_2O_3, SiO_2, SrO, ZnO), and sulfate (SO_3), indicating a more heterogeneous mineralogical structure and depositional history. In contrast, narwhal tusk presents a more uniform Ca–P matrix and may serve as a reference for hydroxyapatite purity.

Previous studies have used an Olympus Vanta M-series handheld XRF spectrometer (Nganvongpanit et al. 2016b) in Geochem2 mode (McLellan, Carrothers & Spicer 2022) performing two 10 s scans per sample surface (5 s high-energy beam + 5 s low-energy beam) to quantify the weight percentages of Ca, P, and light elements (atomic number < 12). This approach has successfully distinguished non-ivory materials such as deer bone and antler from genuine ivory.

However, as observed from both the EDX and XRF analysis results, the EDX data in Table 1 show that walrus tusk is distinctly enriched in magnesium (0.8 wt %) compared to narwhal tusk (0.5 wt %), whereas sodium is slightly higher in narwhal (1.0 wt %) than in walrus (0.8 wt %) but exhibits overlapping ranges between narwhal and walrus tusks, making it unsuitable as a sole discriminant parameter.

All other major elements such as oxygen, carbon, calcium, phosphorus and chlorine exhibit almost identical abundances in both tusks; in particular, their Ca/P ratios (approximately 1.92 for narwhal vs. 1.96 for walrus) fall within the same range, so meaning Ca/P cannot differentiate between the two. However, this analytical approach is conceptually sound. Building upon this methodology, a discrimination strategy based on the Al_2O_3/P_2O_5 ratio is proposed. In the dataset, the Al_2O_3/P_2O_5 ratio for narwhal tusk samples ranges from a minimum of 0.00057 to a maximum of 0.00322, whereas for walrus tusk samples, this ratio ranges from 0.00333 to 0.03445 and a threshold R_0=0.0033 is selected.

Define

$$R = \frac{Al_2O_3(wt\%)}{P_2O_5(wt\%)}$$

Samples with R<0.0033 are classified as narwhal tusk, whereas those with R>0.0033R>0.0033 are walrus tusk. In our dataset there is no overlap across this threshold, yielding a 'zero-error' classification: all narwhal tusk samples fall below 0.0033 and all walrus tusk samples exceed 0.0033. At the same time, the EDX results provided a determination of the magnesium content in the samples, if an extra layer of assurance is desired, one can compute.

Define

$$R_2 = \frac{Mg(wt\%)}{Na(wt\%)}$$

and use a threshold of R2,0≈0.75

If R2<0.75⇒ Narwhal tusk

R2>0.75⇒ Walrus tusk

However, since the aluminum-to-phosphorus ratio showed no overlap between the two sample groups and was based on a larger sample size than the EDX results, it is sufficient for distinguishing the samples, while the magnesium-to-sodium ratio serves only as a supplementary indicator.

MORPHOLOGY, PORE STRUCTURE AND SURFACE CHARACTERIZATION

SEM images provide detailed morphological and pore structure information at the micrometer to nanometer scale, while Raman micro-spectroscopy acquires vibrational spectra from micro-regions, enabling localized surface characterization. In this research, SEM micrographs and Raman spectra are presented together within a single subsection for each representative organic and inorganic constituent, accompanied by their respective spectral peaks. Integrating morphological features and chemical

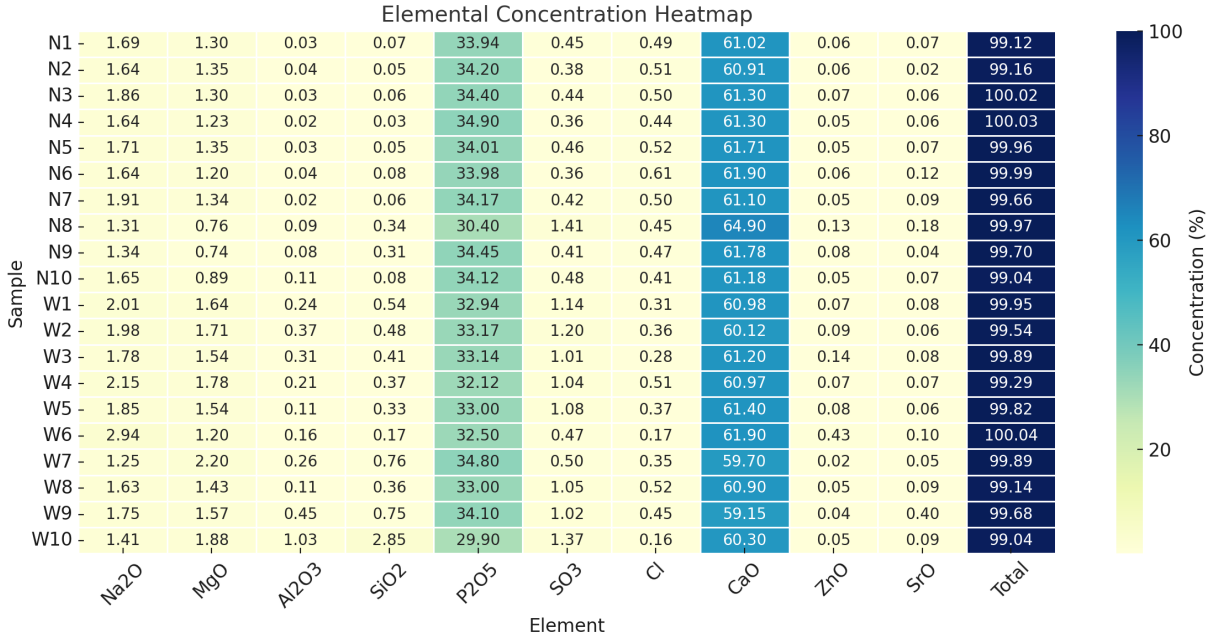

FIGURE 2. XRF elemental concentration heatmap of the samples

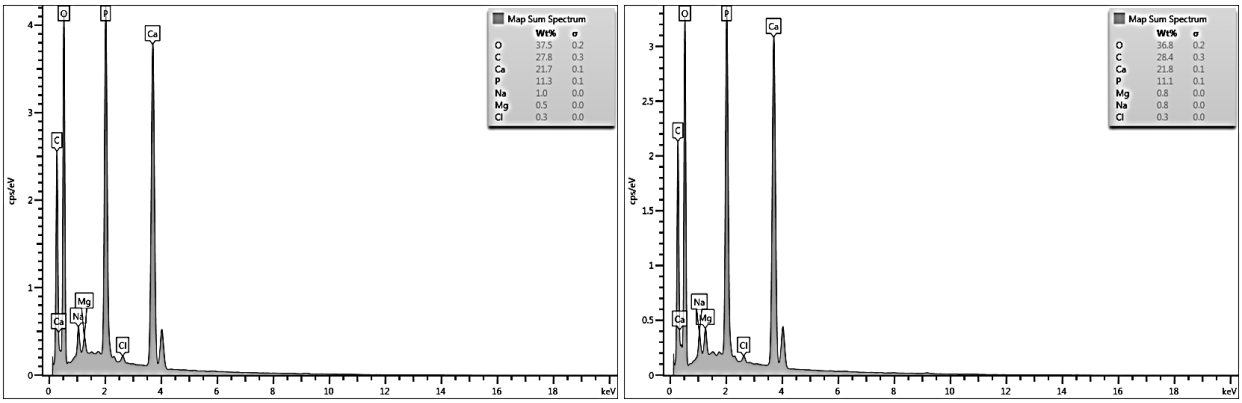

FIGURE 3. SEM-EDX spectrum of representative narwhal sample N6 (left) and walrus, W9 (right)

TABLE 1. Comparative EDX quantitative results for narwhal and walrus tusk

Element	Narwhal tusk (EDX wt %)	Walrus tusk (EDX wt %)	Difference (walrus – narwhal)
O	37.5 ± 0.2	36.8 ± 0.2	–0.7
C	27.8 ± 0.3.	28.4 ± 0.3	+0.6
Ca	21.7 ± 0.1	21.8 ± 0.1	+0.1
P	11.3 ± 0.1	11.1 ± 0.1	–0.2
Na	1.0 ± 0.0	0.8 ± 0.0	–0.2
Mg	0.5 ± 0.0	0.8 ± 0.0	+0.3
Cl	0.3 ± 0.0	0.3 ± 0.0	0.0

bonding data at corresponding locations facilitates a more comprehensive interpretation. Multiple sets of SEM images were obtained for both sample types, as illustrated in Figures 4 and 5.

The SEM image of narwhal tusk shows a well-organized fibrous–crystalline composite structure: elongated, plate-like hydroxyapatite crystals are uniformly embedded along collagen fiber bundles, with fine and evenly distributed pores and a smooth surface, indicating good preservation of the organic matrix and mineral phase in synergy. In contrast, walrus tusk features irregular aggregates of crystalline blocks, macropores, cracks, and secondary precipitates. These characteristics reflect partial degradation of the collagen matrix, followed by weathering, dissolution, and recrystallization processes, resulting in increased crystal dimensions, rougher morphologies, and a significant reduction in structural integrity and alignment (Engel et al. 2022; Unal et al. 2021; Xiang et al. 2024). These microstructural variations observed in the SEM images highlight the contrast between the highly ordered mineral–organic composite framework, consistent with calcium phosphate–based bioapatite, in narwhal tusk and the disrupted structure of walrus tusk.

To further elucidate the microstructural distinctions between narwhal and walrus ivory, a simplified two-dimensional schematic diagram offers an accessible visual comparison that complements the SEM imagery. In the narwhal tusk section (Figure 6, left), parallel, wavy lines denote the organized collagen fiber scaffold, while embedded plate-like forms correspond to elongated hydroxyapatite crystals, highlighting the continuous and well-preserved alignment characteristic of the fibrous–crystalline matrix. In contrast, the walrus tusk section (right) features polygonal domains representing disordered, blocky apatite crystal aggregates. Accompanying cracks and scattered dots symbolize weathering-induced fissures and secondary mineral precipitates, thus capturing the phenomena of matrix loss, recrystallization, and post-depositional alteration observed in aged or diagenetically altered walrus ivory. This schematic (Figure 6) succinctly encapsulates the key microstructural signatures that distinguish the two species' ivory.

SURFACE MOLECULAR STRUCTURE AND CRYSTALLINITY CHARACTERIZATION

Representative samples of narwhal tusk (N4) and walrus tusk (W10) were analyzed using to Raman spectroscopy to determine their molecular compositions. For direct comparison, individual Raman spectra for each sample are shown (Figure 7) along with an overlaid spectrum (Figure 8), allowing precise assessment of both shared and diagnostic vibrational features. This arrangement facilitates integrated interpretation of microstructural and chemical data with morphological observations.

In Figure 7, the right panel depicting the spectrum of walrus tusk (W10), serves as the primary example for spectral assignment and discussion, with emphasis on subsequent correlation to SEM findings. Key vibrational bands are observed: the peaks at 411 cm^{-1} and 617 cm^{-1} correspond to the ν_2 and ν_4 bending modes of the PO_4^{3-} group, confirming a hydroxyapatite lattice structure (Unal et al. 2021). The distinct band at 871 cm^{-1} is attributed to the ν_2 deformation mode of B-type substituted CO_3^{2-}, indicating minor carbonate substitution within the apatite framework. The prominent peak at 961 cm^{-1}, assigned to the ν_1 symmetric stretching of PO_4^{3-}, is a principal marker for hydroxyapatite; its intensity and sharpness reflect the crystallinity of the mineral phase. A minor band at approximately 1317 cm^{-1} is attributable to CH_2 side-chain twisting (Amide III), while the 1608 cm^{-1} peak reflects C=O stretching (Amide I region), highlighting the presence of remnant organic collagen matrix (Morris & Mandair 2011). Collectively, these spectral characteristics indicate that the sample is a composite of highly crystalline hydroxyapatite closely associated with an organic collagen framework. From the left panel of Figure 7 and the overlaid Raman spectra in Figure 8 comparing N4 (red line) and W10 (blue line), notable differences between the two samples can be observed. Most prominently, the intensity of the 961 cm^{-1} peak, corresponding to the ν_1 symmetric stretching mode of PO_4^{3-} - a characteristic feature of hydroxyapatite - differs substantially: N4 exhibits a sharp peak reaching nearly 80 counts, whereas W10 shows a broader peak with a maximum intensity of approximately 25 counts. This indicates that the hydroxyapatite in the narwhal tusk is highly crystalline, while that in the walrus tusk is comparatively disordered.

Comparative analysis using the left panel of Figure 7 and the overlaid spectra in Figure 8 (where N4 is represented by the red trace, W10 by the blue trace) shows pronounced differences between narwhal and walrus tusks. Notably, the 961 cm^{-1} ν_1 peak in narwhal tusk (N4) is sharply defined and reaches a much higher intensity (~80 counts) than the broader, less intense peak in walrus tusk (W10, ~25 counts), indicative of greater mineral crystallinity in narwhal ivory. Additionally, distinct organic-associated bands at 1249, 1443, and 1664 cm^{-1} (corresponding to Amide III, CH_2 bending, and Amide I, respectively) are observed in N4 but are nearly absent in W10. This suggests the retention of collagenous organic matrix in narwhal tusk, while the organic phase in walrus tusk is extensively degraded and/or overprinted by secondary mineralization. These findings are consistent with SEM-based observations of surface weathering and mineral reprecipitation in walrus tusk, providing a coherent picture of compositional and structural divergence between the two marine ivory types.

BIOMINERAL COMPOSITION AND CRYSTALLOGRAPHIC VARIATION

X-ray diffraction (XRD) analysis was employed to show mineralogical and crystallographic variations between narwhal and walrus tusks, which otherwise share substantial

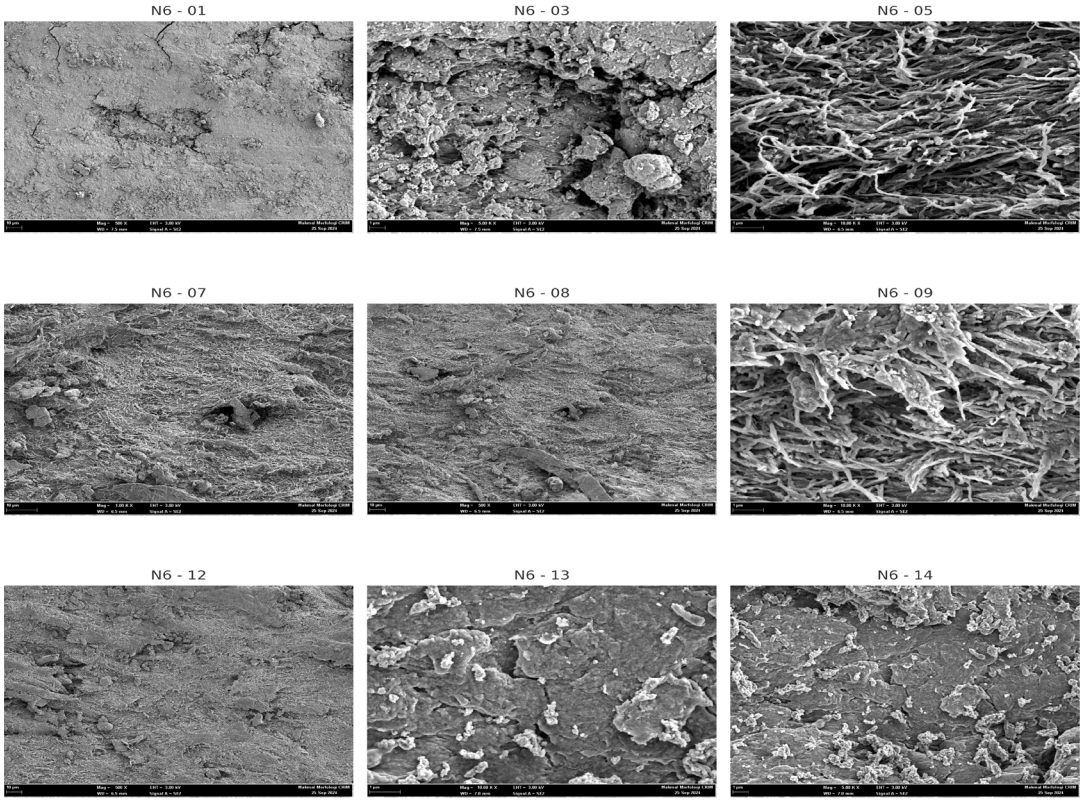

FIGURE 4. Morphology and pore structures of narwhal tusk (N6)

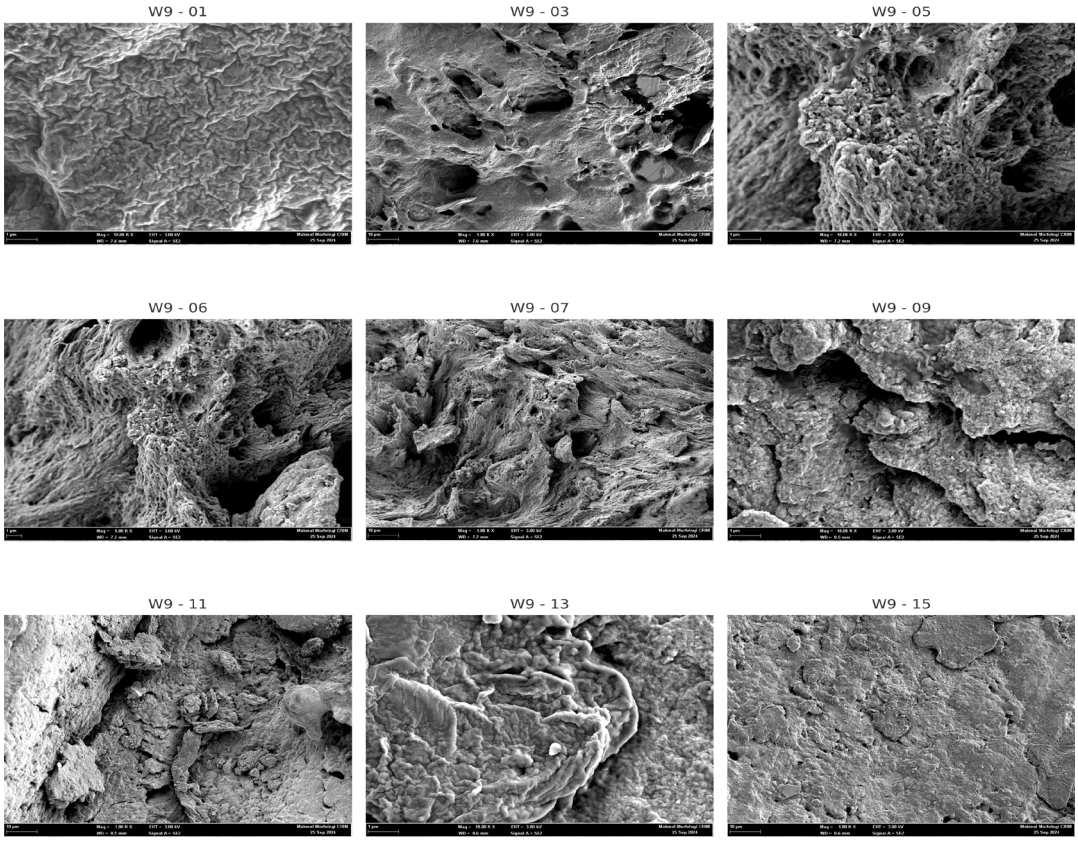

FIGURE 5. Morphology and pore structure of walrus tusk (W9)

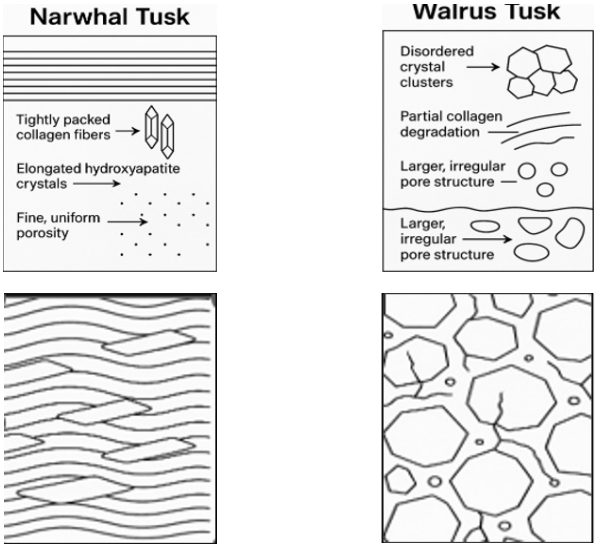

FIGURE 6. Comparative schematic illustration of narwhal and walrus tusk microstructures, highlighting the organized, fibrous–crystalline matrix with fine uniform porosity in narwhal ivory (left) and the disordered crystal clusters, degraded collagen, and larger, irregular pore structures characteristic of walrus ivory (right)

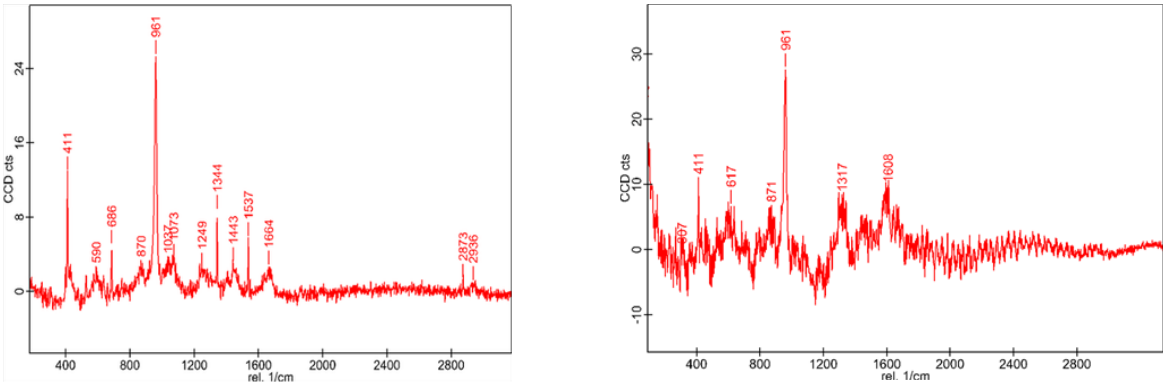

FIGURE 7. Raman spectra of representative narwhal (N4) and walrus (W10) tusks samples

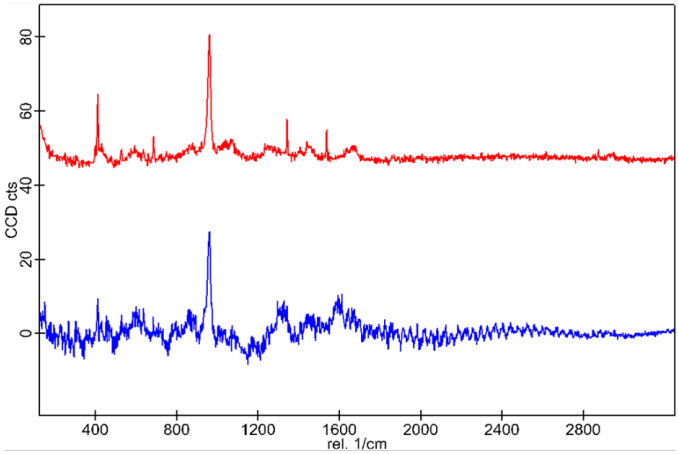

FIGURE 8. Combined Raman spectra of narwhal tusk (N4, red) and walrus tusk (W10, blue)

chemical similarity. Figure 9 displays representative diffraction patterns for narwhal (N1) and walrus (W1) tusk samples, each exhibiting major reflections attributable to apatite phases, alongside subtle peak shifts and minor peaks linked to carbonate and fluoride substitutions. All samples presented characteristic XRD peaks corresponding to hydroxyapatite ($Ca_5(PO_4)_3OH$), confirming calcium phosphate as the primary mineral component. However, inspection of peak positions and profiles suggests the presence of significant carbonate substitution - specifically, partial replacement of PO_4^{3-} by CO_3^{2-} forming carbonate-hydroxyapatite, as indicated by peak shifts in the 30–33° 2θ region and distinct carbonate-related signals. Concurrent fluoride substitution is evidenced by increased intensity around the 26° (002) reflection, which can be attributed to the formation of fluorapatite ($Ca_5(PO_4)_3F$) and associated improvement in crystallinity (Madupalli, Pavan & Tecklenburg 2017).

The main diffraction peaks for both narwhal and walrus tusks generally align, reflecting a common hexagonal apatite structure. Nevertheless, relative peak intensities and detailed pattern features show subtle differences. For example, narwhal samples (N1, N2) exhibit slightly shifted and broader peaks near (211)/(112) reflections, which may result from differences in ionic substitution, especially carbonate content. Higher intensity and sharper peaks in some walrus samples imply larger and better-ordered crystallite domains, while broader peaks in narwhal tusk suggest smaller, more disordered crystallites - potentially reflecting distinct biological or functional requirements.

Quantitative analysis of the patterns shows substantial carbonate-apatite contributions, with both tusk types containing approximately 40% carbonate-substituted hydroxyapatite, although with variations in proportions and crystallinity. Broad peak profiles and elevated backgrounds indicate nanoscale particle size and low crystallinity typical of bioapatite; SEM and EDX data further support these trends, with walrus tusk displaying sharper, more resolved diffraction peaks relative to narwhal tusk. These differences may arise from species-specific biomineralization strategies and environmental influences, rather than diagenetic alteration, as all specimens were well-preserved.

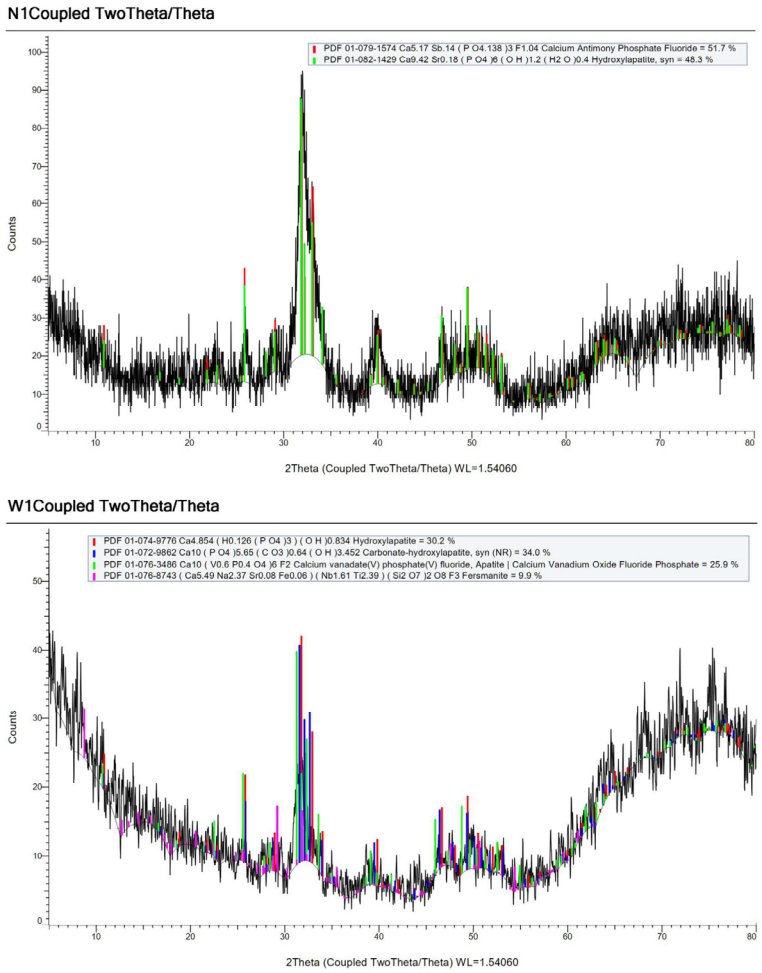

FIGURE 9. XRD patterns of representative narwhal (N1) and walrus (W1) tusks samples

Impurity atom incorporation into the apatite lattice is also showed through XRD. Antimony (Sb) and cadmium (Cd) were uniquely detected in narwhal tusk, while vanadium (V) doping is prominent in walrus tusk. Both types also exhibit strontium (Sr), sodium (Na), and magnesium (Mg) substitution within the crystal lattice (Smičiklas et al. 2010). These elemental signatures likely derive from dietary intake and habitat-specific exposure, and such doping patterns may serve as geochemical markers for forensic discrimination of tusk origin.

CONCLUSIONS

This study employed a comprehensive suite of analytical techniques—including scanning electron microscopy (SEM), X-ray diffraction (XRD), X-ray fluorescence spectroscopy (XRF), and Raman spectroscopy - to systematically characterize and compare the mineralogical, microstructural, and geochemical properties of walrus and narwhal tusks. Several significant findings were obtained: Foremost, a discriminant criterion based on the Al_2O_3/P_2O_5 elemental ratio was established, with a threshold value (R_0) of 0.0033 enabling clear and error-free classification of all analyzed samples. Walrus tusks consistently exhibited ratios above this threshold, while narwhal tusks remained below it, demonstrating robust, non-destructive differentiation. This approach holds substantial practical utility for rapid species identification, facilitating enforcement actions against illegal trade and supporting the safeguarding of cultural heritage.

Integrated SEM and Raman analyses showed fundamental differences in microstructure and mineral crystallinity. Narwhal tusks exhibited a highly organized architecture, defined by uniformly aligned collagen fibers tightly integrated with elongated hydroxyapatite crystals and preserved primary collagen matrices - indicative of advanced biomineralization. In contrast, walrus tusks displayed disordered crystal aggregations, partially degraded collagen frameworks, extensive secondary mineral deposition, and greater porosity and cracking, reflecting distinct environmental adaptations and biological functions. From an organic gemmological perspective, these microstructural attributes suggest narwhal tusk artifacts possess superior density, oiliness, and tactile quality compared to those derived from walrus tusk.

XRD analysis confirmed that carbonate-substituted hydroxyapatite constitutes the dominant mineral phase in both tusk types. Subtle but meaningful distinctions in crystallinity and elemental substitution were observed: narwhal tusk apatite featured higher carbonate content and generally smaller crystal sizes, while walrus tusk crystals had greater overall crystallinity and more extensive fluoride substitution, likely influenced by functional roles and environmental ion exchange mechanisms.

In conclusion, the research provides a reliable, evidence-based framework for the identification of marine ivory, underpinned by biomineral composition, microstructural, and geochemical criteria. The Al_2O_3/P_2O_5 ratio emerges as a compelling diagnostic marker with direct enforcement potential and implications for both market regulation and heritage conservation. Future work will target broader sample and geographic ranges, leveraging advanced analytical methodologies to elucidate the impacts of ecological variation and nutrition on tusk biomineralization, further refining the scientific foundation for marine ivory identification.

ACKNOWLEDGEMENTS

We gratefully acknowledge Assoc. Prof. Dr. Azimah Hussin for her expert guidance and support throughout the research. Sincere thanks to the anonymous donors from indigenous communities in the Russian Far East for providing the walrus and narwhal tusk specimens. Appreciation is extended to the Faculty of Science and Technology, Universiti Kebangsaan Malaysia, and to external laboratories for technical assistance. Special thanks to family and friends, including Zhong Songyang, Yin Shiwei, and Jiang Minghao for their encouragement and support.

REFERENCES

Darwent, C.M. & LeMoine, G.M. 2021. Pre-Inuit walrus use in Arctic Canada and Greenland, c.2500 BCE to 1250 CE. In *The Atlantic Walrus,* edited by Keighley, X., Olsen, M.T., Jordan, P. & Desjardins, S. Academic Press. pp. 99-120.

Dąsal, M., Smakosz, A., Kurzyna, W. & Rudko, M. 2021. "Unicorn horn" drugs in the medical and pharmaceutical culture of Europe. *Farmacja Polska* 77(2): 84-94.

Edwards, H.G.M. & O'Connor, S. 2012. Archaeological ivories: A challenge for analytical Raman spectroscopy. In *Analytical Archaeometry*, edited by Edwards, H. & Vandenabeele, P. The Royal Society of Chemistry. pp. 449-467.

Engel, W., Gennari, R.F., Ferreira, C. & Rizzutto, M. 2022. Ivory characterization using portable vibrational spectrometry. *Southern Brazilian Journal of Chemistry 2021 Virtual Conference*. pp. 1-4.

Grandfield, K., Chattah, N.L.T., Djomehri, S., Eidelmann, N., Eichmiller, F.C., Webb, S., Schuck, P.J., Nweeia, M. & Ho, S.P. 2014. The narwhal (*Monodon monoceros*) cementum-dentin junction: A functionally graded biointerphase. *Proceedings of the Institution of Mechanical Engineers , Part H: Journal of Engineering in Medicine* 228(8): 754-767.

Hemer, K.A., Willmott, H., Evans, J.E. & Buckley, M. 2023. Ivory from early Anglo-Saxon burials in Lincolnshire - A biomolecular study. *Journal of Archaeological Science: Reports* 49: 103943.

Hoelzig, H., Muenster, T., Blanke, S., Kloess, G., Garmasukis, R. & Koenig, A. 2020. Ivory vs. osseous ivory substitutes - Non-invasive diffractometric discrimination. *Forensic Science International* 308: 110159.

Kiladze, A.B. & Chernova, O.F. 2018. Data on the angular characteristics of the spiral structure of the narwhal tusk. *Data in Brief* 20: 1700-1703.

Locke, M. 2008. Structure of ivory. *Journal of Morphology* 269(4): 423-450.

Madupalli, H., Pavan, B. & Tecklenburg, M.M.J. 2017. Carbonate substitution in the mineral component of bone: Discriminating the structural changes, simultaneously imposed by carbonate in A and B sites of apatite. *Journal of Solid State Chemistry* 255: 27-35.

Mamaladze, M.T. & Ustiashvili, M.G. 2010. Theoretical and practical principles of dentinogenesis: Hypotheses and confirmed clinically reality. *Georgian Medical News* 186: 22-28.

McLellan, M.J., Carrothers, K.L. & Spicer, A.M. 2022. Investigating the utility of a handheld X-ray fluorescence (XRF) device as a field test for suspected ivory. *Forensic Science International: Animals and Environments* 2: 100041.

Morris, M.D. & Mandair, G.S. 2011. Raman assessment of bone quality. *Clinical Orthopaedics and Related Research* 469(8): 2160-2169.

Nganvongpanit, K., Buddhachat, K., Klinhom, S., Kaewmong, P., Thitaram, C. & Mahakkanukrauh, P. 2016a. Determining comparative elemental profile using handheld X-ray fluorescence in humans, elephants, dogs, and dolphins: Preliminary study for species identification. *Forensic Science International* 263: 101-106.

Nganvongpanit, K., Buddhachat, K., Piboon, P. & Klinhom, S. 2016b. The distribution of elements in 48 canine compact bone types using handheld X-ray fluorescence. *Biological Trace Element Research* 174(1): 93-104.

Sastri, C.S., Banerjee, A., Sauvage, T., Courtois, B. & Schuhmacher, T. 2013. Fluorine determination in different types of ivory by PIGE technique. *Journal of Radioanalytical and Nuclear Chemistry* 298(1): 311-315.

Sims, M.E., Baker, B.W. & Hoesch, R.M. 2011. Tusk or bone? An example of ivory substitute in the wildlife trade. *Ethnobiology Letters* 2: 40-44.

Silaev, V.I., Smoleva, I.V., Filippov, V.N., Shanina, S.N., Khazov, A.F., Makeev, B.A., Kiseleva, D.V., Fokina, A.K. & van der Plicht, J. 2025. Pleistocene Walrus on the Pechora River: Mineralogical and geochemical data and paleoecological reconstructions. *Doklady Biological Sciences* 520(1): 49-59.

Smičiklas, I., Dimović, S., Šljivić, M., Plećaš, I., Lončar, B. & Mitrić, M. 2010. Resource recovery of animal bones: Study on sorptive properties and mechanism for Sr^{2+} ions. *Journal of Nuclear Materials* 400(1): 15-24.

Su, X.W. & Cui, F.Z. 1999. Hierarchical structure of ivory: From nanometer to centimeter. *Materials Science and Engineering C* 7(1): 19-29.

Tranchant, L., Müller, K., Lemasson, Q., Pichon, L., Schöder, S., Conard, N.J. & Reiche, I. 2023. Improved discrimination of biogenic and diagenetic elements in Palaeolithic mammoth ivory and bone from Hohle Fels Cave in the Swabian Jura of Southwestern Germany. *Quaternary International* 660: 4-12.

Unal, M., Ahmed, R., Mahadevan-Jansen, A. & Nyman, J.S. 2021. Compositional assessment of bone by Raman spectroscopy. *Analyst* 146(24): 7444-7470.

Xiang, S., Jiang, L., Wang, Y., Li, S., Jiang, L., Wang, N., Zhu, L., Zhao, L. & Hong, J. 2024. Research on the micro-structure and water effect of excavated ivory from sacrificial pit No.7 at the Sanxingdui Ruins. *Heritage Science* 12: 411.

*Corresponding author; email: haqqim@ukm.edu.my